Geomechanics for Energy and the Environment 40 (2024) 100599

Contents lists available at ScienceDirect

Geomechanics for Energy and the Environment

journal homepage: www.elsevier.com/locate/gete

# Assessing swelling-induced damage in shale samples during triaxial testing

E. Crisci [a], R. Ewy [b], A. Ferrari [c,d], S.B. Giger [e,*]

[a] Nesol, Numerical Engineering Solutions, Lausanne, Switzerland
[b] Tufts University, MA, USA
[c] École Polytechnique Fédérale de Lausanne, EPFL, Lausanne, Switzerland
[d] University of Palermo, Engineering Department, Palermo, Italy
[e] National Cooperative for the Disposal of Radioactive Waste (NAGRA), Wettingen, Switzerland

A R T I C L E I N F O

*Keywords:*
Shales
Opalinus Clay
Damage
Triaxial testing
Low effective confinement
Swelling
Fissuring

A B S T R A C T

In shale testing, understanding the impact of effective stress and saturation conditions is crucial for accurate material behaviour assessment and parameter determination. In some cases, saturation in triaxial testing starts at low effective stress before ramping up for shearing. However, when in contact with water (or saline water), shales are prone to swelling, particularly at low effective stress levels, which can induce fissures and alter material properties. This study investigates the influence of fluid saturation strategies and stress/pressure variations on the mechanical behaviour of shales, particularly under low effective confinement. Building upon the comprehensive testing campaign (>140 tests) in Crisci et al. (2024), additional tests were conducted on Opalinus Clay shale, focusing on sample saturation methods and loading histories before shearing. The conditions under which tested specimens experience damage were detected through diagnostic indicators such as differences in stress path and lower strength and stiffness compared to intact specimens with identical basic properties. Micro CT scanning confirms that damage is related to the development of fissures. The volumetric changes in specimens were quantified throughout the testing phases and thresholds for tolerable strains and effective stresses, specific to this material, were established. Comparative analysis with Opalinus Clay from shallower depths and other shales globally revealed consistent findings. Notably, it is shown that, for all shale types analyzed, a linear failure envelope emerges in the low to intermediate effective stress regime when filtering out "damaged" specimens. This suggests that non-linear failure envelopes observed in some cases may stem from exposing specimens to low effective stress before shearing.

## 1. Introduction

Shales and claystones (hereafter referred to simply as shales) are very fine-grained sedimentary geomaterials with elevated clay-mineral content, and with distinct bedding planes and variable degree of cementation. For these geomaterials, the evaluation of the effective stress and of the degree of saturation during testing is fundamental, since the contact with fluids and pore fluid pressure variations highly impact the behaviour. It is particularly relevant therefore to understand the rock-fluid interaction and adopt adequate testing procedures to prevent misestimation of the hydromechanical parameters[17,9,11,3].

Dedicated testing procedures have been developed and adopted in particular for Opalinus Clay shale[14,15,18,4].

Saturation and testing of shales is sometimes done at low effective confinement, to either mimic the in-situ field conditions (e.g. in excavation applications) or to avoid exceeding the maximum effective stress to which the shale was subjected[9].

Clay-based geomaterials are generally subjected to non-negligible volumetric strain induced by saturation changes, both during drying (i.e. desiccation cracks) and during wetting. In geomaterials with a certain degree of cementation (such as shales and claystones), cycles of environmental changes cause degradation of the cementation, causing fissuring[1,17,20]. It is therefore needed to understand what minimal stress and maximum strain conditions the material can sustain during saturation without experiencing severe changes in its hydromechanical parameters.

A large experimental campaign was conducted on Opalinus Clay in Northern Switzerland in the context of site selection for a deep geological repository, thanks to an intense deep boreholes campaign (hereafter referred to as TBO), adopting previously validated testing protocols, and

* Correspondence to: National Cooperative for the Disposal of Radioactive Waste – Nagra, Hardstrasse 73, Postbox, Wettingen CH-5430, Switzerland.
*E-mail address:* silvio.giger@nagra.ch (S.B. Giger).

https://doi.org/10.1016/j.gete.2024.100599
Received 16 May 2024; Received in revised form 4 September 2024; Accepted 16 September 2024
Available online 20 September 2024

demonstrating a very high degree of reproducibility of the test results[4].

In this contribution, additional tests are reported and compared to those from the large campaign in[4]. A set of dedicated tests was conducted to investigate the role of the fluid saturation strategy and effective stress variation throughout all phases of testing on the potential degradation of the samples' mechanical properties (damage). Samples were prepared with a cylinder's axis perpendicular to the bedding orientation (S-samples). These tests included slight variations in the testing procedure adopted by Crisci et al.[4], namely for the sample saturation phase and the changes of effective confining stress before shearing.

Imaging techniques were employed to evaluate the microstructure of a sample during swelling. Evaluation of the results amongst comparable samples tested with different testing strategies revealed the latter's effect on the parameter determinations. As will be demonstrated, part of these additional tests experienced some degree of mechanical damage and were therefore excluded from Crisci et al.[4], but contributed to the understanding of critical stress and strain conditions to induce damage to the sample.

## 2. Material and methods

### 2.1. Context and sample extraction

The Opalinus Clay in present-day northern Switzerland was deposited in a shallow epicontinental sea during the early Middle Jurassic. The burial history is complex and characterized by two major subsidence periods in the early Cretaceous and early Paleogene, separated and followed by two major uplift periods[16]. The maximum temperature of the Opalinus Clay in its geological history was approximately 90–100º C, and the estimated maximum burial depth was approximately 2000 m, hence much deeper than the current extraction depth of cores (Table 1). The estimated maximum burial depth corresponds to an estimated maximum vertical effective stress in the order of 25 MPa.

Cores designated for geomechanical testing were treated so as to minimize potential handling effects on laboratory analyses, adopting special conditioning methods. The exposure time to the atmosphere was kept to the minimum time (less than 20 minutes) required to allow core documentation, then the cores were immediately inserted into PVC tubes and axially constrained with bar clamps. Epoxy (Sikadur-52) was used to fill the small annulus (nominal 3.2 mm) between the 95 mm nominal diameter core and the PVC tube to avoid core water loss, and it was verified that the temperature rise from the curing of the epoxy was well below the in-situ temperature from which the core was sourced, to avoid any potential thermal effect. X-ray computed tomography of all cores from Opalinus Clay were analysed to assess integrity and heterogeneity within the cores.

From the core scan, sections of the cores to be tested were identified. The specimens' extraction was carefully performed to minimize water content loss during the operation and during sample storage prior to testing. All involved laboratories used a rotary core barrel and hydrocarbons as cooling fluids during the drilling of the specimens. The size of the cylindrical testing specimens was either 25 mm in diameter and 50 mm in length (sample ID starting with A or B in Table 2) or 19 mm in diameter and 38 mm in length (sample ID starting with C in Table 2). More information can be found in[4].

### 2.2. Material properties

In deep borehole locations, Opalinus Clay generally presented a bulk density in the range 2.48 – 2.59 g/cm$^3$. Natural water content (of extracted samples) and porosity were in the ranges 3.1 – 6.5 wt% and 7.1 – 13.8 % respectively, while clay mineral content varies within the range 32 – 71 wt%.

The initial properties of the tested samples discussed in this contribution (additional tests and tests from corresponding sections from[4]) are reported in Table 1. The table includes the borehole name, the number of samples considered from each borehole (in parenthesis), the corresponding sample depth, the clay mineral content, and the initial (as-prepared) water content, bulk density and porosity of the samples. The latter properties are reported in terms of median, minimum and maximum values.

### 2.3. Testing procedure

#### 2.3.1. Methodology for mechanical testing in triaxial conditions

The main characteristics of the triaxial tests discussed in this paper are given in Table 2. Two different procedures were used for triaxial compression testing, referred to here as the 'conventional' and the 'alternative' procedures[18]. Both procedures consist of the following test phases: i) sample saturation, ii) diagnostic control of saturation by small increments in confining stress (Skempton-B, referred to as B-steps hereafter), iii) consolidation (or reverse consolidation) to target effective stress, and iv) undrained (or drained) shear phase. The main difference between the procedures is in the methods used to achieve sample saturation. There is also often a difference in the consolidation step in that the conventional procedure usually imposes an effective stress decrease while the alternative procedure usually imposes an effective stress increase; however, there are exceptions to this as discussed in the following.

A brief description of the conventional procedure is as follows, and additional details can be found in[18]. This procedure uses a preserved sample with as-cut water content. Artifical pore water (see Appendix, Table B, for the recipe) is brought into contact with the sample (in the triaxial rig), while the axial and radial stresses are independently increased to maintain zero strain during the saturation process. For S-orientation samples, this usually results in axial effective stress values of 20–35 MPa, and in radial effective stress values of 10–25 MPa. Radial stress is brought to a value equal to axial stress prior to B-steps. Depending on the target effective stress value at the start of shearing, the

**Table 1**
Properties and initial conditions of tested samples.

| Borehole (number of samples) | Sourcing depth of samples | | Clay mineral content | Initial water content | Initial bulk density | Initial porosity |
|---|---|---|---|---|---|---|
| | m | | wt% | wt. - | g/cm$^3$ | - |
| TRU1_1 (8) | 836.6 - | median | 54.2 | 0.0461 | 2.53 | 0.111 |
| | 925.2 | min | 52.2 | 0.0432 | 2.51 | 0.107 |
| | | max | 63.7 | 0.0525 | 2.53 | 0.122 |
| BOZ1_1 (14) | 546.6 - | avg | 59.9 | 0.0475 | 2.51 | 0.117 |
| | 649.2 | min | 45.5 | 0.0379 | 2.49 | 0.099 |
| | | max | 61.4 | 0.0520 | 2.56 | 0.129 |
| MAR1_1 (7) | 608.3- | avg | 57.4 | 0.0477 | 2.52 | 0.117 |
| | 647.8 | min | 48.0 | 0.0453 | 2.48 | 0.105 |
| | | max | 66.6 | 0.0646 | 2.55 | 0.133 |
| BOZ2_1 (15) | 504.6–566.3 | avg | 53.0 | 0.0447 | 2.54 | 0.107 |
| | | min | 48.0 | 0.0351 | 2.50 | 0.089 |
| | | max | 70.3 | 0.0579 | 2.57 | 0.129 |

**Table 2**
List of tests and main testing characteristics. p'$_0$ is the initial mean effective stress at the start of shearing. Procedure: C=conventional; A= alternative. [1] Compression to higher stress level (higher than the end of saturation and of the shearing target) – variation to the alternative and conventional procedure. [2] Data from[4]. Details of all other test results can be found in[5,6,7,8].

| ID | Borehole | Depth m | p'$_0$ MPa | Procedure | Saturation | Additional compression[1] | Stress path |
|---|---|---|---|---|---|---|---|
| A4_TRU1_1[2] | TRU1–1 | 836.6 | 8 | C | Isochoric | No | CTCU |
| B2_TRU1_1[2] | TRU1–1 | 851.9 | 10 | C | Isochoric | No | CTCU |
| B7_TRU1_1[2] | TRU1–1 | 875.8 | 7 | C | Isochoric | No | CTCU |
| C4_TRU1_1 | TRU1–1 | 895.1 | 4 | A | Desiccator, isostatic compression | No | CTCU |
| C5_TRU1_1[2] | TRU1–1 | 895.1 | 13 | A | Desiccator, isostatic compression | No | CTCU |
| A8_TRU1_1[2] | TRU1–1 | 903.4 | 8 | C | Isochoric | No | CTCU |
| A11_TRU1_1[2] | TRU1–1 | 903.4 | 8 | C | Isochoric | No | CTC |
| A10_TRU1_1[2] | TRU1–1 | 925.2 | 5 | C | Isochoric | No | CTCU |
| C13_BOZ1_1[2] | BOZ1–1 | 546.6 | 7 | A | Desiccator, isostatic compression | No | CTCU |
| C1_BOZ1_1[2] | BOZ1–1 | 546.7 | 13 | A | Desiccator, isostatic compression | No | CTCU |
| C3_BOZ1_1[2] | BOZ1–1 | 546.7 | 7 | A | Desiccator, isostatic compression | No | CTCU |
| C5_BOZ1_1[2] | BOZ1–1 | 568.5 | 13 | A | Desiccator, isostatic compression | No | CTCU |
| C7_BOZ1_1 | BOZ1–1 | 568.5 | 7 | A | Desiccator, isostatic compression | No | CTCU |
| C12_BOZ1_1[2] | BOZ1–1 | 568.5 | 7 | A | Desiccator, isostatic compression | No | CTC |
| A1_BOZ1_1[2] | BOZ1–1 | 584.9 | 6 | C | Isochoric | No | CTCU |
| A2_BOZ1_1[2] | BOZ1–1 | 584.9 | 6 | C | Isochoric | No | C TC |
| A8_BOZ1_1 | BOZ1–1 | 649.0 | 7 | C | At target effective stress (2 MPa) | No | CTCU |
| A5_BOZ1_1[2] | BOZ1–1 | 649.0 | 7 | C | Isochoric | No | CTCU |
| A6_BOZ1_1[2] | BOZ1–1 | 649.0 | 13 | C | Isochoric | No | CTCU |
| A9_BOZ1_1[2] | BOZ1–1 | 649.0 | 7 | C | At target effective stress (10 MPa) | No | CTCU |
| A10_BOZ1_1[2] | BOZ1–1 | 649.2 | 7 | C | Isochoric | No | CTCU |
| A11_BOZ1_1[2] | BOZ1–1 | 649.2 | 7 | C | At target effective stress (2 MPa) | Yes (to p'=20 MPa) | CTCU |
| C5_MAR1_1[2] | MAR1–1 | 608.3 | 13 | A | Desiccator, isostatic compression | No | CTCU |
| C7_MAR1_1 | MAR1–1 | 608.3 | 7 | A | Desiccator, isostatic compression | No | CTCU |
| B1_MAR1_1[2] | MAR1–1 | 617.4 | 7 | C | Isochoric | No | CTCU |
| B2_MAR1_1[2] | MAR1–1 | 617.4 | 5 | C | Isochoric | No | CTC |
| C1_MAR1_1[2] | MAR1–1 | 647.8 | 13 | A | Desiccator, isostatic compression | No | CTCU |
| C3_MAR1_1 | MAR1–1 | 647.8 | 6 | A | Desiccator, isostatic compression | No | CTCU |
| C11_MAR1_1[2] | MAR1–1 | 647.8 | 5 | A | Desiccator, isostatic compression | No | CTC |
| C11_BOZ2_1 | BOZ2–1 | 504.6 | 7 | A | Desiccator, isostatic compression | Yes (to p'=17 MPa) | CTCU |
| C6_BOZ2_1[2] | BOZ2–1 | 504.7 | 13 | A | Desiccator, isostatic compression | No | CTCU |
| C5_BOZ2_1 | BOZ2–1 | 504.8 | 7 | A | Desiccator, isostatic compression | No | CTCU |
| C12_BOZ2_1[2] | BOZ2–1 | 504.8 | 7 | A | Desiccator, isostatic compression | Yes (to p'=17 MPa) | CTCU |
| C1_BOZ2_1 | BOZ2–1 | 504.9 | 7 | A | Desiccator, isostatic compression | No | CTCU |
| C2_BOZ2_1 | BOZ2–1 | 504.9 | 13 | A | Desiccator, isostatic compression | No | CTCU |
| C7_BOZ2_1[2] | BOZ2–1 | 504.9 | 7 | A | Desiccator, isostatic compression | Yes (to p'=17 MPa) | CTCU |
| C9_BOZ2_1[2] | BOZ2–1 | 504.9 | 13 | A | Desiccator, isostatic compression, active saturation at constant effective stress (25 MPa) | Yes (to p'=25 MPa) | CTCU |
| B12_BOZ2_1 | BOZ2–1 | 519.3 | 7 | A | Desiccator, active saturation at constant effective stress (7 MPa) | No | CTCU |
| B1_BOZ2_1[2] | BOZ2–1 | 519.3 | 7 | C | Isochoric | No | CTCU |
| B2_BOZ2_1[2] | BOZ2–1 | 519.3 | 13 | C | Isochoric | No | CTCU |
| C3_BOZ2_1 | BOZ2–1 | 566.3 | 7 | A | Desiccator, isostatic compression | No | CTCU |
| C4_BOZ2_1[2] | BOZ2–1 | 566.3 | 13 | A | Desiccator, isostatic compression | No | CTCU |
| C8_BOZ2_1[2] | BOZ2–1 | 566.3 | 7 | A | Desiccator, isostatic compression | Yes (to p'=17 MPa) | CTCU |
| C10_BOZ2_1[2] | BOZ2–1 | 566.3 | 7 | A | Desiccator, isostatic compression, active saturation at constant effective stress (25 MPa) | Yes (to p'=31 MPa) | CTCU |

consolidation step usually entails a reduction in effective stress; this results in some sample expansion.

Three tests adopted a variation on the conventional procedure in which saturation took place under constant total stresses to a target effective stress value, allowing some swelling to intentionally occur. The rest of the test proceeded as per the conventional procedure, with saturation verification, consolidation to target mean effective stress and shearing.

In the alternative procedure, the sample water content is adjusted by equilibrating it at a specific relative humidity in a desiccator before mounting the sample. This phase, referred to as preconditioning throughout the paper, lasted until significant changes in water content were no longer observed. The pore line is filled (in most cases) with non-aqueous fluid, and sample saturation is achieved through undrained isostatic compression (see[15,18]). This is then followed by B-steps to confirm saturation. By design, the effective stress at the end of B-steps is less than the target for the start of shearing, so drainage and sample compression occur during consolidation. Relative humidity (RH) values typically between 92 % and 96 % were used in order to achieve sufficiently high pore pressure during undrained isostatic compression. The samples were not restrained from swelling.

Four tests used a variation on the alternative procedure, in which the samples were consolidated to high effective stress (17 MPa) and then unloaded prior to shearing. Two tests used a combined alternative-conventional procedure (with artificial water in the pore line): undrained isostatic compression did not generate sufficient pore pressure (due to lower RH); the samples were actively saturated at an effective stress of ~25 MPa, followed by B-steps and unloading to the target for shearing. In one case, the sample was initially equilibrated to high relative humidity, then saturation was completed in the rig, at constant isotropic stress.

### 2.3.2. Testing program

The large testing program[4] focused on the detailed geomechanical characterization of Opalinus Clay, including material variability and anisotropy, as a basis for site comparison. Here, additional tests from the same cores are discussed, focusing on the impact of volumetric changes on the test specimen at low effective stress (Table 2). A subset of the tests reported by Crisci et al.[4] is also listed in Table 2 as they are used for comparison with the new tests. Detailed information on mechanical test results of all tests not covered by Crisci et al.[4] can be found in borehole-specific and publicly available data reports[5,6,7,8].

Test specimens from the same depth were cored adjacent to each other, thereby minimizing potential effects from variable facies or mineralogy.

Table 2 reports the list of samples taken into consideration in this contribution. The table includes the ID, the borehole and depth of sample recovery, the initial mean effective stress for shearing p′0, the adopted testing procedure (conventional or alternative, the saturation strategy and the recompression after saturation and before shearing), and the stress path (CTC= conventional triaxial compression drained, or CTCU for undrained test).

### 2.3.3. Fissure detection during preconditioning

To investigate the effect of the preconditioning on the sample mechanical response, a dedicated analysis was conducted. Two samples were plugged from the same slice of a core. One sample (B1_BOZ2_1) was then tested following the conventional procedure. The second sample was hydrated in the desiccator, then saturation was completed in the rig (B12_BOZ2_1, Table 2).

Sample B12_BOZ2_1 was scanned with microcomputed tomography (μCT) at the end of sample coring. Then, the ends were ground for flatness, dimensions and mass were measured, and the sample was put in a desiccator to hydrate. The humidity in the desiccator was controlled by a saturated brine solution of Potassium phosphate monobasic ($KH_2PO_4$) which provides a relative humidity of 96 % at 22°C.

Sample dimensions and mass were periodically registered, and after 33 days of hydration a second set of μCT scans was made. The sample was then returned into the desiccator for another 12 days before testing to compensate for potential water loss during scanning. The results allow for a qualitative comparison of the images before and after hydration.

## 3. Results

### 3.1. Saturation and consolidation

### 3.1.1. Volumetric strain and water content changes

Samples tested adopting the alternative procedure were subjected to an increase in saturation due to RH equilibrium in a desiccator, outside of the triaxial cell. This allowed measurement of the increase in weight (i.e. in water content) and in dimensions (i.e. volumetric strain) before putting the sample in the triaxial rig. Furthermore, deformation in the rig was measured at all times, and allowed determination of the strain to which the samples were subjected due to the different testing procedures (as summarised in Table 2). For samples subjected to RH increments in the desiccator, water content measurements before and after the RH equilibration are reported in Fig. 1 (Table A in the appendix). Water content increments ranged between 0.3 – 0.8 wt%, with an average of 0.5 wt%.

In Fig. 2, the axial effective stress versus axial swelling strain at saturation of a set of samples from BOZ1–1 depth 649 m is shown. These 6 samples were extracted from the same section of the core, so heterogeneity among them is negligible. Samples were saturated in the rig at either isochoric conditions (strain is kept as close as zero as possible) or under constant confining stresses. As stress is reduced, the amount of swelling increases exponentially. Similar observations were made also in Delage and Belmokhtar[9] on Opalinus Clay samples from borehole Lausen.

Volumetric strains for samples tested with the conventional and alternative procedures are shown in Fig. 3. Reported values correspond to the end of equilibration in the desiccator or the end of saturation in the rig (depending on the testing procedure) and at the beginning of shear, after the consolidation and/or reverse-consolidation phases.

During equilibration in the desiccator, the samples experienced volumetric swelling strains of approximately −1 % (median value), with

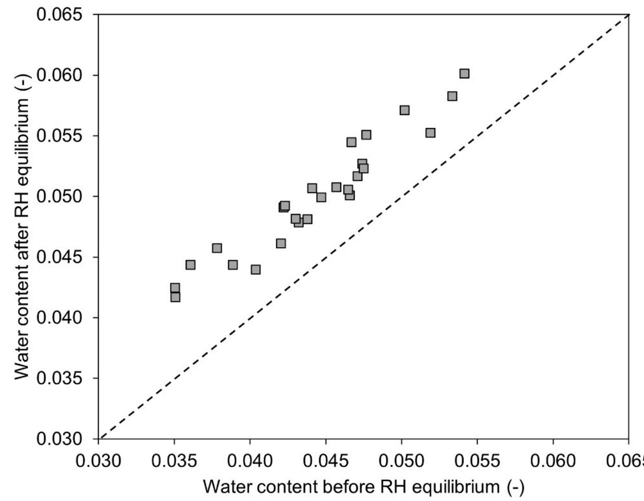


**Fig. 1.** Water content before and after equilibrium in the desiccator for samples tested with alternative procedure, showing the increase in water content in all samples.

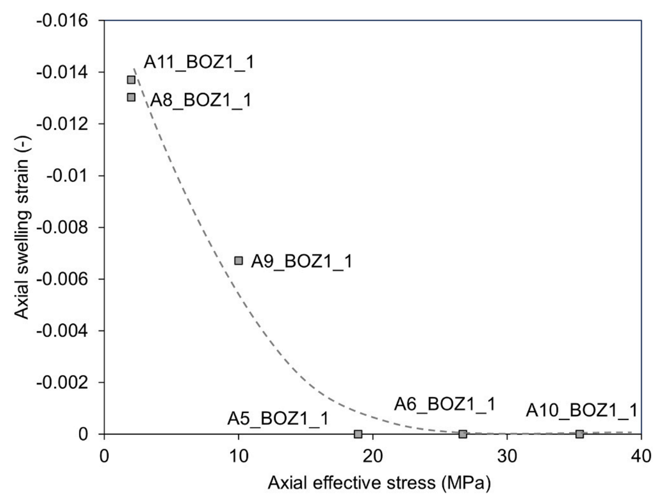


**Fig. 2.** Axial effective stress versus axial swelling strain during saturation indicating significantly increased swelling under low axial effective stress conditions.

peaks as high as −1.5 %. The volumetric swelling strains (due to saturation) were partially recovered in the cell during pre-shear compression; however, in some cases, volumetric strain at the beginning of the shear phase remained negative (swelled samples) with peaks up to −1.4 %.

For samples saturated in the cell, in most cases, the saturation was conducted in isochoric conditions (strains remain zero in this phase). High confining stresses, up to 35 MPa, were necessary to maintain the sample deformation close to zero. These stress levels were in most cases higher than the current in-situ stress, and also potentially higher than the maximum past effective stress to which the material was subjected. However, past testing campaigns on Opalinus Clay revealed that initial mean effective stress (up to 50 MPa) had no impact on the measured mechanical properties[15]. Also, Ewy et al.[10] showed that yield stress for claystones is usually 2–3 times greater than maximum past stress. Therefore the relatively high confining stresses necessary to maintain isochoric conditions during saturation are not expected to have any relevant adverse effect on the material properties.

In the following test phases, samples were unloaded to target confinement, which resulted in swelling strain (Fig. 3, top). At the

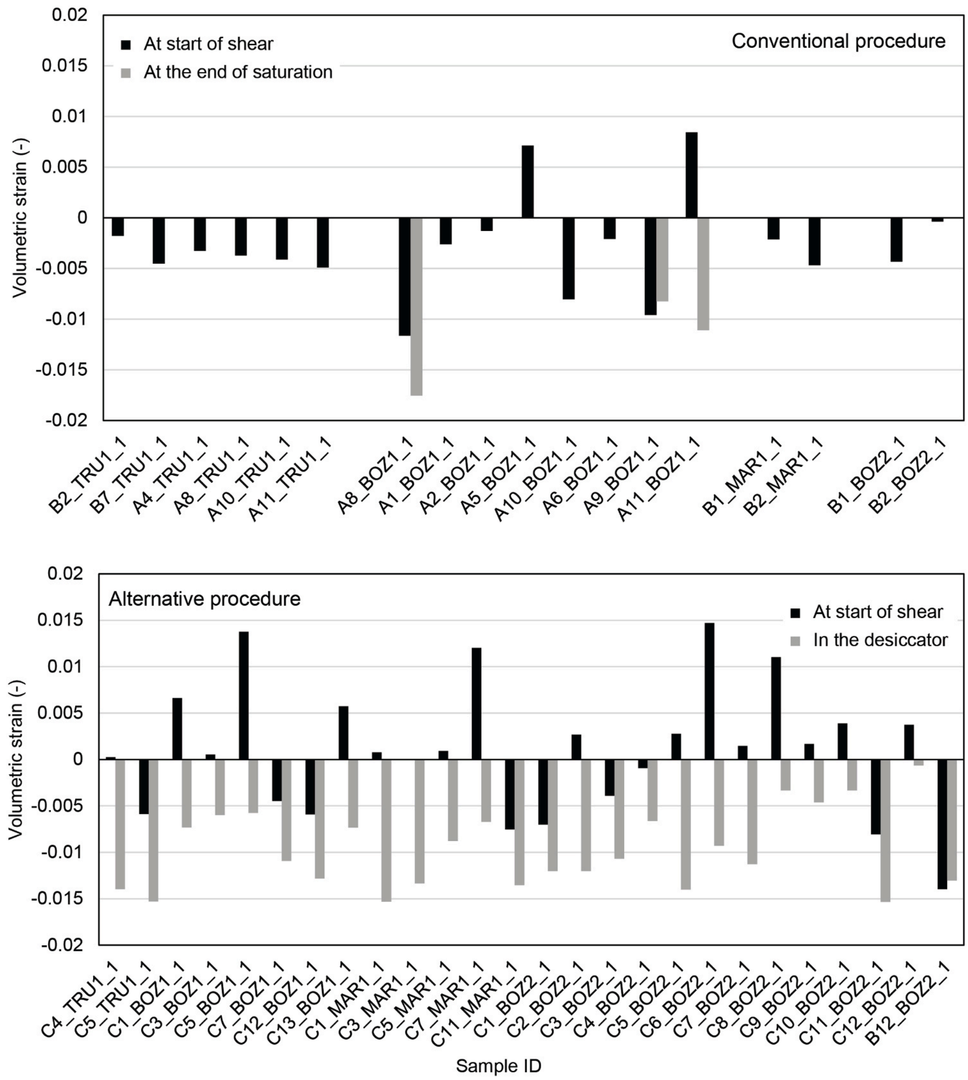


**Fig. 3.** Volumetric strain (compression positive) for samples tested with the conventional (top) and alternative (bottom) procedures. Values at the end of saturation (in the rig or the desiccator) and at the beginning of shear, after consolidation and reverse-consolidation phases. Zero-strain conditions during saturation result in a non-visible data value.

beginning of the shear phase, the samples experienced a median volumetric swelling of −0.35 %, with peaks reaching −1.16 %.

### 3.1.2. Micro CT results

The evolution of the volumetric strains and of the water content of sample B12_BOZ2_1 are shown in Fig. 4. At day 33, the sample was extracted from the desiccator, wrapped in plastic and a second μCT scan was performed. Despite the precaution in limiting water loss, water content slightly decreased during this operation, and a minor contraction (~0.1 %) in volumetric strain was observed, as shown in Fig. 4. After the scan, the sample was placed again in the desiccator and let to equilibrate for an additional 12 days. Both the water content and the volumetric deformation recovered (and even exceeded) the previous loss.

Two vertical sections of the sample are shown in Fig. 5, and their comparison before and after RH equilibrium is highlighted.

The first scan (Fig. 5a and c) allowed to verify the initial presence of fissures. One fissure was already macroscopically visible in the untrimmed sample, and it can also be seen on the CT scans(arrow in Fig. 5a and c). No other fissures were detected. Subsequently, the edges were cut (bottom and top dashed lines in Fig. 5), and the 50 mm long specimen could be prepared from the fissure-free region. After end-

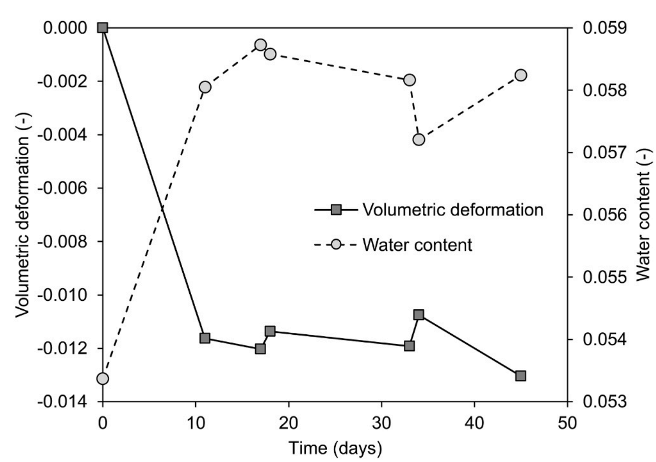


**Fig. 4.** Water content and volumetric strain evolution during equilibration of sample B12_BOZ2_1 in the desiccator at RH=96 %. Note volumetric expansion of approximately 1.2 % within first 10 days.

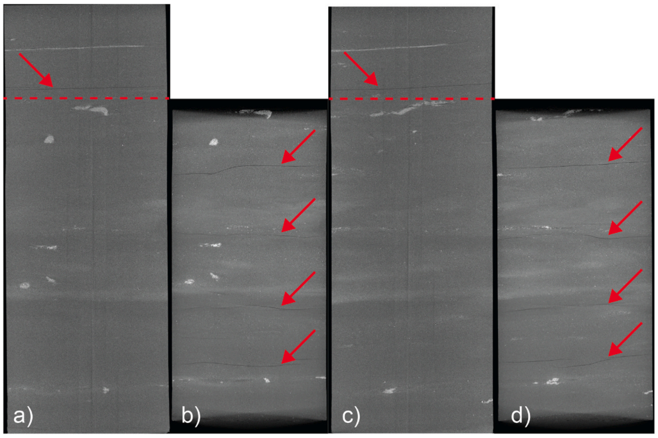


**Fig. 5.** Vertical slices of CT scans of sample B12_BOZ2_1 before (a, c) and after equilibration (b, d) to RH=96 %, demonstrating the development of new, sub-horizontal fissures(red arrows). Dashed red lines indicate the locations where the initial cored section was cut into the final sample.

trimming, no visible fissures were identified. The second scan done after 33 days of equilibration in the desiccator shows (Fig. 5b and d), that during the water content increment, in the absence of any physical constraint to the expansion, at least four micro fissures formed. The observation is in agreement with previous findings in clay rocks (e.g.,[1,2,19]). In previous studies, it was observed that fissures during swelling tend to originate at the boundary between heterogeneous components of the samples, e.g. at the boundary between clay matrix and inclusions of quartz or other minerals. The clay matrix absorbs water and tends to swell. For non-swelling minerals, the reduction of suction (i.e. effective stress) induces minor swelling, related to the effective stress decrease. The incompatibility in the deformations generates localised stress that causes the formation of cracks.

### 3.2. Shearing phase

In this section, the analysis of some sets of tested samples is provided, highlighting the differences in the hydromechanical response to differences in the saturation and testing procedures.

Fig. 6 and Fig. 7 shows four sets of samples. The figures report on the left, the stress path and on the right the stress-strain response during the shearing phase. In the p′-q plane, the condition of zero radial effective stress is reported with a dashed line. Both on the stress path and stress-strain curves, the three stress levels for the following conditions are marked: (i) the maximum deviator stress (qMax), (ii) the maximum pore pressure (UwMax) and (iii) the maximum AB value (ABMax), with AB being the ratio of the increment in pore pressure to the increment in deviator stress (the total radial stress is maintained constant during the shearing phase).

Fig. 6 shows, in the top panels, the results from tests C5_BOZ2_1, C11_BOZ2_1 and C12_BOZ2_1 (all tested with the alternative procedure) starting shearing from $p'_0$=6–7 MPa. Samples C5_BOZ2_1 and C11_BOZ2_1 experienced the highest volumetric swelling (-1.5 %) of all the cores from that borehole equilibrated in the desiccator. The samples were tested with the alternative procedure, however, C11_BOZ2_1 and C12_BOZ2_1 were subjected to a re-compression to higher confinement, before unloading to target $p'_0$ (Table 2). During re-compression, sample C11_BOZ2_1 partly recovered this −1.5 % volumetric expansion in the desiccator, resulting in a net volumetric expansion of about −0.8 % at the beginning of the shear phase, while C12_BOZ2_1 was in a state of compressive strain (Fig. 3). The stress path of test C5_BOZ2_1 is curving slightly more to the left than the other two tests, indicating the development of higher pore water pressure. Both tests with very high initial expansion (C5_BOZ2_1 and C11_BOZ2_1) exhibit UwMax at a lower deviator stress than C12_BOZ2_1 and clearly a lower qMax value. Also, effective radial confinement at max pore pressure is low (curves close to the zero radial effective stress line). Results are reported in the Appendix, Table A. Both samples C5_BOZ2_1 and C11_BOZ2_1 showed lower peak shear strength compared to the corresponding sample C12_BOZ2_1, which generally experienced small deformation both upon saturation and in the rig.

Tests C1_BOZ2_1, C2_BOZ2_1, C7_BOZ2_1, C9_BOZ2_1 (Fig. 6 bottom panels) were tested by adopting the alternative procedure ($p'_0$= 6–7 MPa for C1_BOZ2_1 and C7, $p'_0$=13 MPa for C2_BOZ2_1 and C9_BOZ2_1). Samples C7_BOZ2_1 and C9_BOZ2_1 were subjected to recompression in the rig to confinement higher than the target for shearing, then unloaded to target confinement (Table 2).

The first three samples experienced swelling deformation during equilibration in the desiccator <-1 %. This volumetric swelling strain was only partially recovered in the following compression phase. The samples C1_BOZ2_1 and C2_BOZ2_1 developed higher pore pressure during shearing, reaching lower effective radial confinement at max pore pressure, than the analogous C7_BOZ2_1 and C9_BOZ2_1, and overall achieving a lower peak shear strength. With the exception of the very early shearing phase, their stress-strain curve showed a softer response and achieved the peak at higher deformation, and lower strength.

For tests B1_BOZ2_1 and B12_BOZ2_1 (the latter used to perform μCT scans), conventional and alternative procedures were adopted, respectively (Table 2). The stress path and stress-strain responses are shown in Fig. 7, top panels. Sample B12_BOZ2_1 showed a higher pore pressure development in the early phase of the shearing, which reached a peak in correspondence to the max shear strength. The stiffness of the response, with the exception of the early phase of shearing, resulted in being lower than the sample B1_BOZ2_1. Also, maximum shear strength in test B12_BOZ2_1 was followed by a phase in which shearing continued at approximately stable deviator stress before softening (e.g. post peak deviatoric stress decrement) occurred. The shear strength of the B12_BOZ2_1 sample was overall 20 % lower than sample B1_BOZ2_1.

In the bottom panel of Fig. 7, results from tests A10_BOZ1_1, A11_BOZ1_1, A5_BOZ1_1, A8_BOZ1_1 and A9_BOZ1_1 are shown. These samples were subjected all to the conventional procedure, but three were saturated adopting a constant confining stress (instead of zero-strain) during saturation: A8_BOZ1_1 and A11_BOZ1_1 were saturated at an effective mean stress of 2 MPa, while A9_BOZ1_1 was at p′=10 MPa (see Fig. 2). In test A11_BOZ1_1, the sample was also loaded to higher confinement (20 MPa) and then unloaded to target confinement for shearing. The only sample showing lower strength, higher pore pressure development and peak strength reached at the same time as maximum pore pressure is test A8_BOZ1_1, which swelled during saturation up to −1.8 %, and did not recover most of the deformation at the time shearing started (~-1 %). Samples A9_BOZ1_1 and A11_BOZ1_1 did not show significant differences with the other two tests, suggesting that the 10 MPa confinement during saturation and the reloading to 20 MPa were sufficient to prevent or recover any potential effect of saturation swelling.

The same diagnostic analysis, based on the stress path and stress-strain evolution was conducted on all the samples.

## 4. Discussion

### 4.1. Damaged samples

Some common responses are observed in the stress path and stress-strain evolution of samples that showed low strength:

– These samples tend to develop higher pore pressure during shearing (stress path deviating to the left).
– Peak strength is often reached shortly after the maximum pore pressure is achieved, and in some cases, once the peak is achieved,

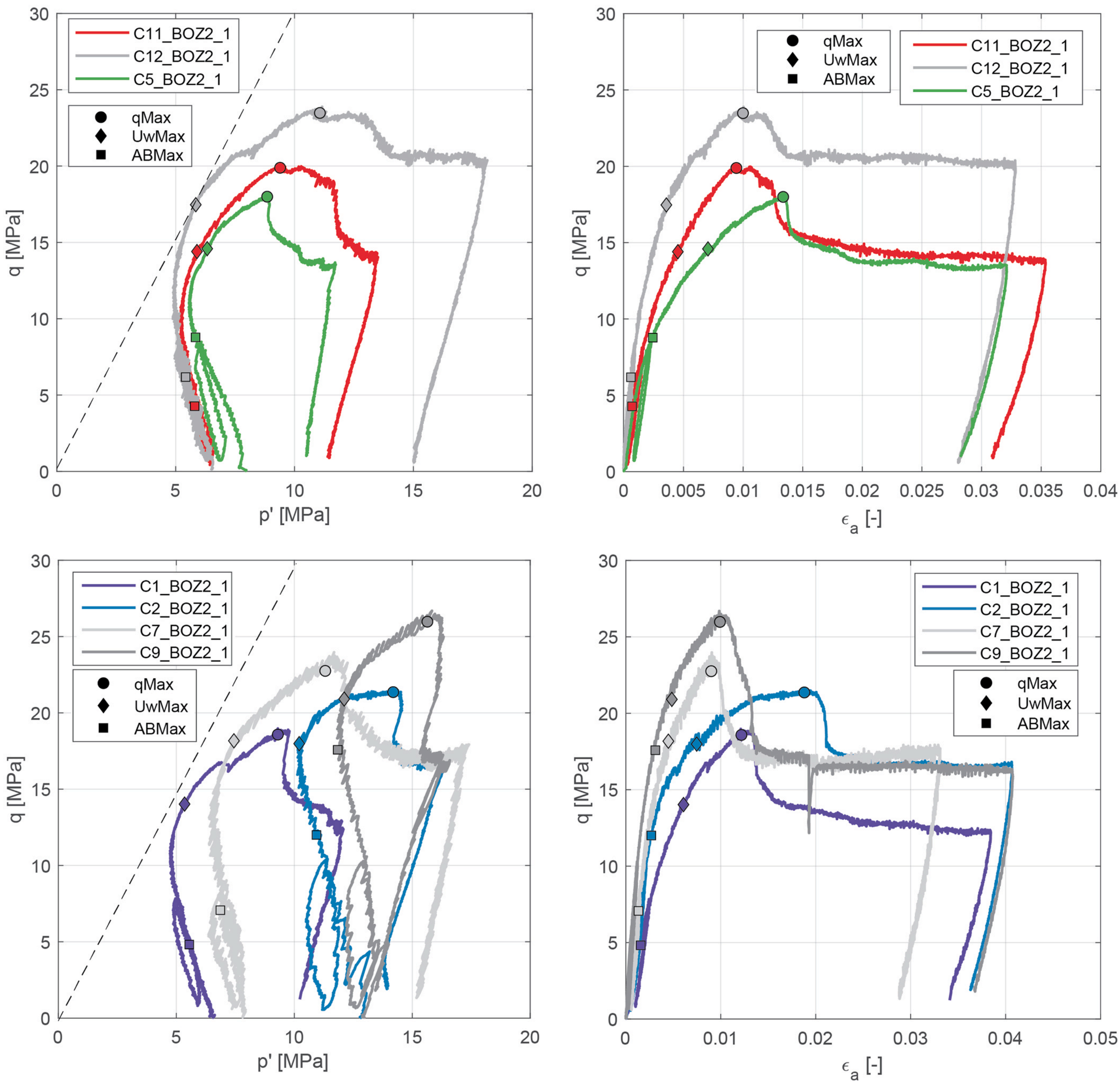


**Fig. 6.** Stress path (left) and stress-strain response for two groups of samples (top and bottom) in BOZ2–1. Dashed 3:1 line indicates the zero radial effective stress. Coloured lines denote tests with high volumetric expansion (more than 1 %) in the desiccator prior to the shear phase, in comparison to test results of Crisci et al.[4] in Grey with nearly identical cores but volumetric expansion typically less than 1 %.

the stress-strain curve evolves maintaining a relatively constant value of deviator stress, for some deformation, before experiencing softening and reaching post-peak values.

– From the stress-strain curves, a softer response is observed during shearing, i.e. the slope of the curve is generally lower, in particular once deviating from the initial linear response.
– Peak strength, or post-peak softening for samples whose curve has a relatively flat evolution around the peak, is achieved at higher axial strain. This confirms the general "softer" response of the samples.

At least two of the above aspects can be observed in each result that showed low strength. Those results are hereafter classified as damaged samples, in contrast with twin undamaged samples. In some cases, the difference in the mechanical response between the damaged and undamaged case is minimal, nonetheless, the lower shear strength is visible. Results for all samples are compiled in Table A in the Appendix.

Fig. 8 reports the values of axial effective stress and radial effective stress for the samples listed in Table 2 at the condition of peak shear stress (maximum q). The results are grouped into two subsets. The red diamonds highlight samples that showed lower strength (damaged) than other test results, from the same tested core sections. Samples ID is reported for each of those.

Table 3 summarises the number of tests for each testing procedure (and variation) and those that yielded damaged samples. The procedures that allowed sample swelling, and in particular that did not include reloading after the saturation, yielded the highest number of damaged samples.

Isochoric saturation was effective to avoid sample damage during the

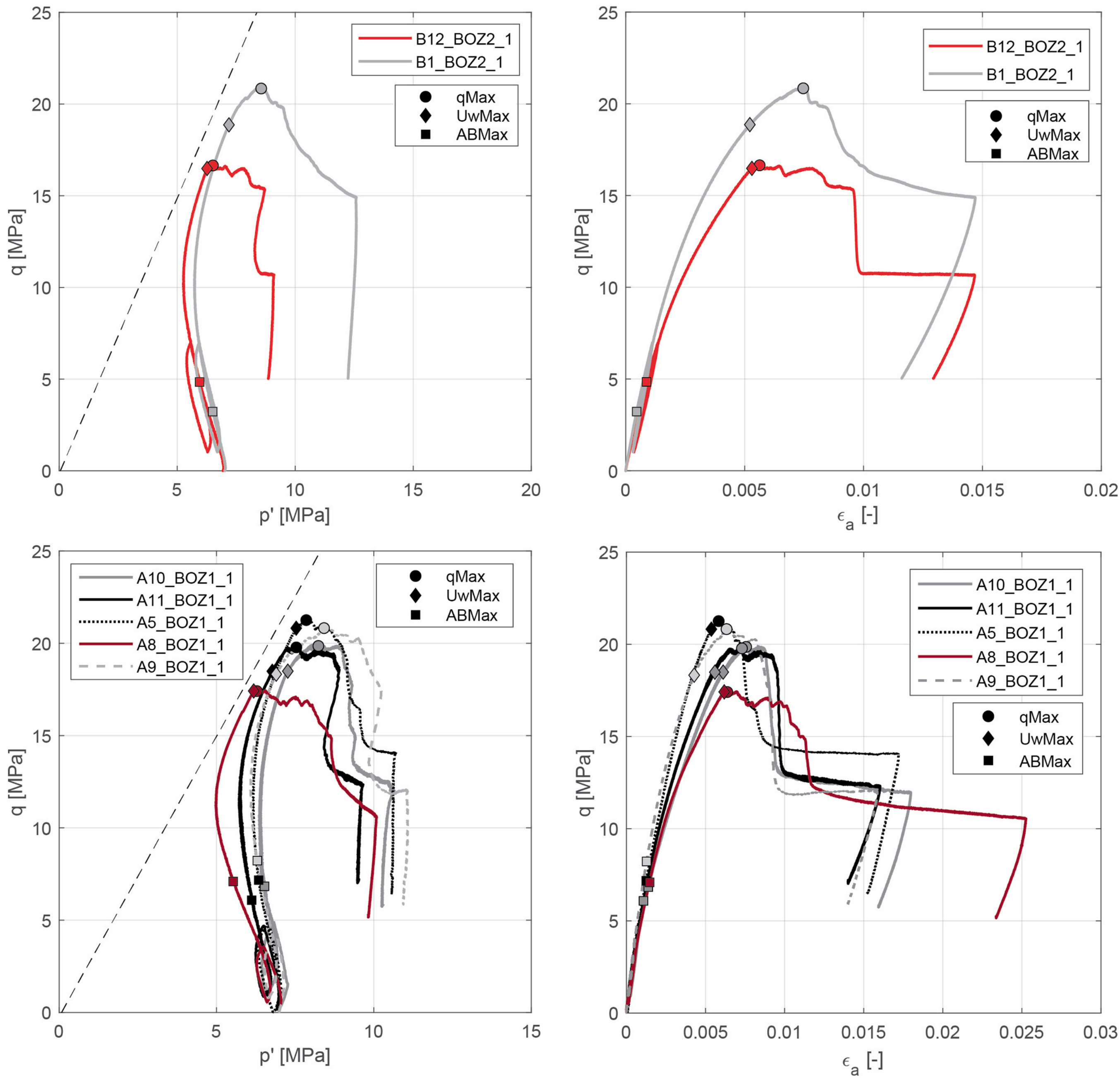


**Fig. 7.** Stress path (left) and stress-strain response for two groups of samples (top and bottom) in BOZ2–1 and BOZ1–1. Dashed 3:1 line indicates the zero radial effective stress. Coloured and Black lines denote tests with high volumetric expansion (more than 1 %) in the desiccator or the rig prior to the shear phase, in comparison to test results in Grey with nearly identical cores but volumetric expansion typically less than 1 %.

early phase of testing. The downside is that it can lead to high stress applied to the sample.

The alternative procedure is known to generate reliable results, and undamaged samples, when low effective stresses are not targeted. Achieving high pore water pressure (low effective stress) through undrained isostatic compression generally requires that water be added during RH equilibration, especially for stiff or deep shales. This water content increase can cause significant volume strain in some cases.

### 4.2. Stress and strain history

The information from Section 3.1 on the deformation experienced by the sample during the preparation and testing phase, are here combined with the results obtained during shearing (Section 3.2). It is observed that (Fig. 9): samples that showed low strength are those that (i) experienced higher swelling strain during the saturation phase(s) and that (ii) at the beginning of shearing had not (or only partially) recovered the swelling. Fig. 9 presents the volumetric strain at the end of preconditioning/saturation versus the volumetric strain at the start of shear, for samples classified as undamaged and damaged. An indication of the stress history is provided by the marker color of each point, which indicates the minimum radial effective stress achieved during shearing. In most cases, during shearing, the pore pressure increment was sufficient to drive the effective confinement of the sample below 1 MPa. The effect of fissures, formed during saturation (Section 3.1.2), might be minimal if the confining pressure is high enough to keep the fissures tight, e.g. fissures might be the weak point for macrofracturing initiation, but are not expected to drive the failure mechanism.

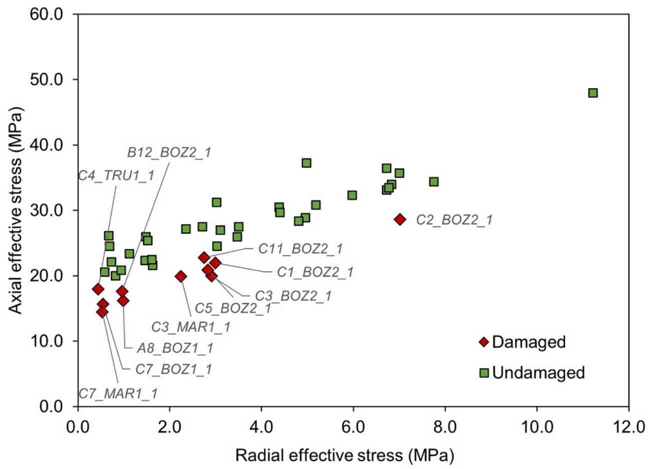


**Fig. 8.** Axial effective stress at failure plotted versus radial effective stress, confirming that tests with high volumetric expansion prior to shear and slightly different stress paths during shear also result in lower strength. These tests are identified as damaged and labelled in the figure.

**Table 3**
Summary of the procedures adopted for sample testing and resulting number of low strength (damaged) samples.

| Procedure | Main testing characteristic | Number of tests | Damaged |
|---|---|---|---|
| Conventional (18) | Isochoric saturation | 15 | 0 |
| | Non-isochoric saturation | 3 | 1 |
| Alternative (26) | Without reload | 19 | 9 |
| | Re-load to p′=15–31 MPa, then unloading | 7 | 1 |

In summary, damaged samples are identified when (i) they experienced high swelling strain during saturation, and (ii) where the strains were not recovered during the test phases before the shearing, and (iii) when they were not reloaded in the cell before shearing (ratio[f] $p'_{max}/p'_0$ is close to 1) or (iv) which achieved negligible confinement (< 1 MPa) during shearing.

### 4.3. Comparison with the larger database

The results are here compared to the larger dataset in Crisci et al.,[4]. Fig. 11 shows, in the top panel, the peak shear strength of samples in the axial versus radial effective stress plane. Damaged samples are highlighted with a red marker line. Median, minimum and maximum regression lines from Crisci et al.,[4] are also reported. It is highlighted that the damaged samples lie along or below the minimum regression line.

Post-peak shear strength, obtained once deviatoric stress stabilised is reported in Fig. 11, bottom panel, in terms of normal effective stress versus shear stress along the observed failure plane. In terms of post-peak stress, the damaged samples (red marker line) are in line with the results of undamaged samples, and no difference can be observed. This observation can be interpreted by considering that the damage to the samples due to volumetric deformation will principally act in degrading the bonding/cementation among particles within the material. Consistent with the development of fissures during excessive swelling (Section 3.1), this is expected to have an impact on the peak material strength. At post-peak, shearing is localised in the shear band, where the alteration of the material has already degraded most if not all the cementation in the material. As such, the damage in the early phase of testing does not impact the result in the post-peak phase.

Elastic undrained moduli are shown in Fig. 11, and compared damaged samples (red marker line) to the database in Crisci et al.,[4]. It is observed that the damaged samples tended to have an elastic modulus in

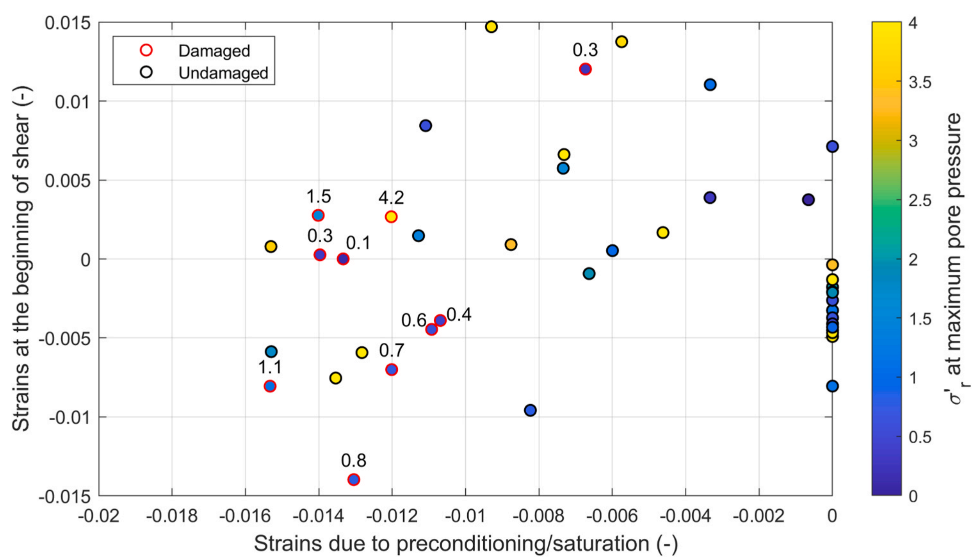


**Fig. 9.** Breakdown of the volumetric expansion into the saturation / preconditioning phase and the following phases before the start of shear. Colour code in circles denote the effective minimum radial stress during shearing (at max pore pressure). Samples with a red marker line indicate the samples defined as damaged in Fig. 8, and the labels specify the effective radial stress value when maximum pore pressure was achieved. Note clustering of damaged samples for strains during preconditioning/saturation <-0.01.

On the other hand, if limited to no stress is applied, the fissures remain open and represent a preferential driver for the failure surface, e.g. potentially leading to lower strength. For samples in which the volumetric swelling deformations were limited during the early phases of testing, it is worth noting that small confinement (<1 MPa) during shearing is not associated with low strength.

the lower range compared to the rest of the results. Nonetheless, no clear distinction can be made between damaged and undamaged samples. As

[f] Ratio of effective mean stress achieved prior to shear phase ($p'_{max}$) vs. effective mean stress at the start of shear ($p'_0$), see Table A in the Appendix.

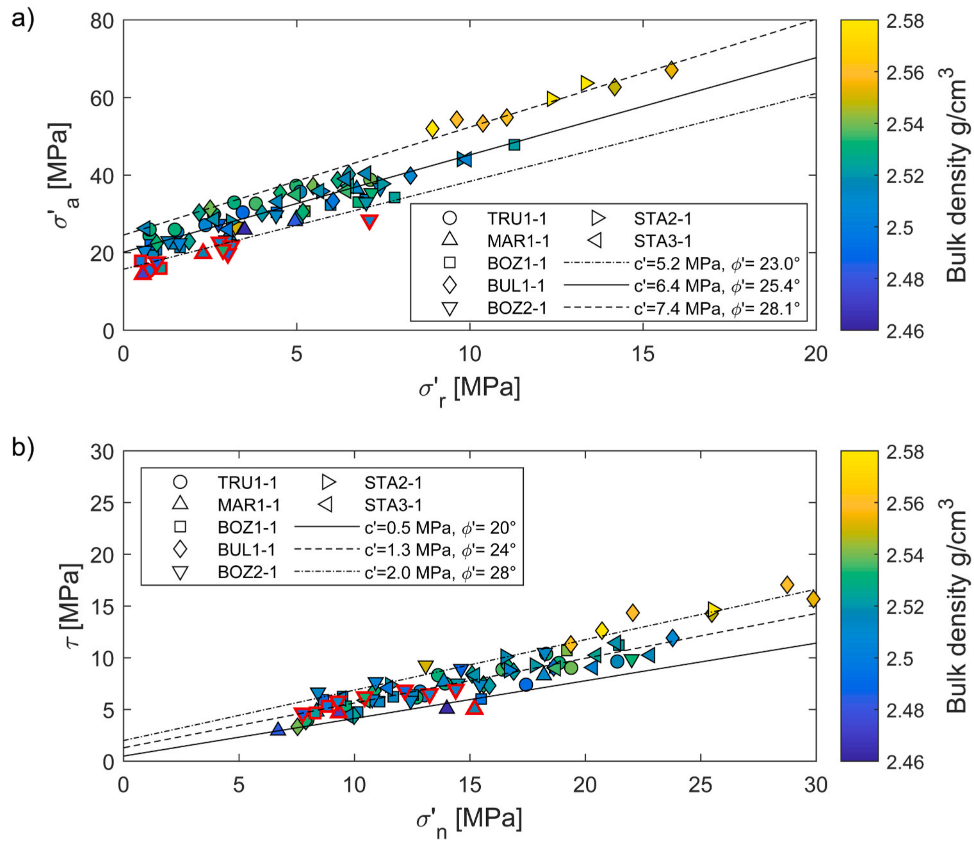


**Fig. 10.** Peak (above) and post-peak (below) shear strength for samples loaded perpendicular to the bedding direction (S-samples). For peak shear strength, the damaged samples (highlighted with a red marker line) line up below the larger database of Crisci et al.,[4]. For post-peak shear strength, the damage is no longer relevant and results cannot be distinguished from the larger database. Note: post-peak shear strength is expressed as shear stress vs. effective normal stress ($\sigma'_n$) to account for orientation of dominant slip surface.

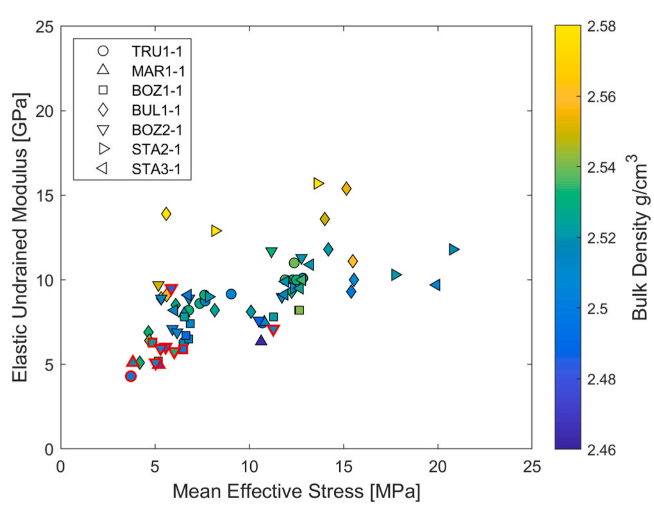


**Fig. 11.** Elastic undrained modulifor samples loaded perpendicular to the bedding direction (S-samples). With one exception, damaged samples (red marker line) again cluster on the low side, consistent with observations on peak strength.

shown in Section 3.2, the stiffness of damaged samples in the early phase of shearing did not show significant difference from the undamaged samples. Yet, with continuous shearing, a softer response was observed in most cases. In this second phase though, the non linear sample response is also associated to an irreversible, plastic response.

### *4.4. A flow chart to anticipate damage effect in Opalinus Clay from TBO*

The observations of the previous section can be condensed into a flow chart, to classify whether a sample is potentially subjected to high or small damage effects, depending on the evolution of stress and strain during testing (Fig. 12).

If limited swelling occurred during saturation (in particular, volumetric strain is >-1 %) or the initial swelling was compensated by compression during the following phases, resulting in a volumetric strain >0.5 % at the beginning of shearing, the sample had small or no effect of damage. It is worth noting that the deformations at the beginning of shearing are impacted by performing a re-compression stage.

In case the swelling was only partially recovered, the confinement seems to play a major role. If the minimum radial effective stress during shearing is higher than 1.5 MPa, generally small or no damage is obtained; lower radial effective stress means the sample is likely to show signs of damage behaviour. The proposed scheme gives guidance in identifying the main factors driving the damage response. Nonetheless, the response of individual samples might differ from the above-mentioned categorisation. Differences in the degree of diagenesis and cementation of the specific sections might be relevant, or higher clay content may better accommodate the swelling strain. Also, recompression to higher effective stress prior to shearing may increase the interlocking of grains across fissures, thereby reducing damage effects of swelling strains even though they are not completely erased.

The values of the threshold identified for Opalinus Clay samples from the TBO are not expected to be valid for shales in general. The reader is referred to Sections 4.5 and 4.6 for the discussion on other shales.

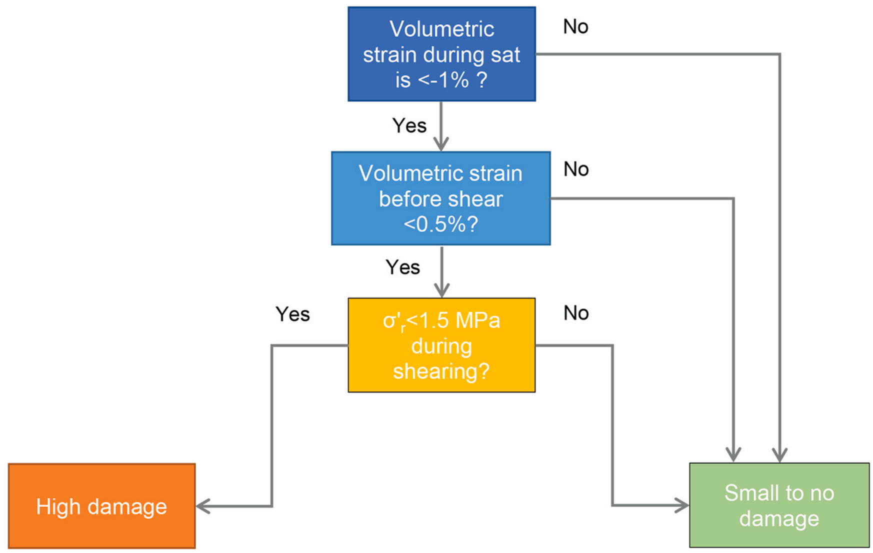


**Fig. 12.** Flow chart to categorise the risk of damage of a tested sample based on the testing procedure and stress and strain history.

### 4.5. Opalinus Clays from shallower locations

Samples of Opalinus Clay from the Mont Terri underground laboratory[18] were tested with the same procedures as those in this paper. In Mont Terri, Opalinus Clay is at a shallower depth (approximately 300 m). Samples were put in desiccators at RH 96–98 %. While the deformations were not measured, the average water content increment was limited to 0.05–0.25 wt%. This is about 5 times lower than what is observed in the TBO. Samples from Mont Terri were subjected to a small unload due to extraction, i.e. the negative pore pressure generated during unloading (and the consequent potential desaturation) is limited compared to the samples extracted from the deep boreholes (500–1000 m). Therefore, the initial saturation conditions of the Mont Terri samples are expected to be closer to full saturation. For Mont Terri samples, an initial RH (or native activity) of cored samples of 94 %-95 % was measured. This further confirms that even though subjected to very high RH, the shales experienced a limited amount of swelling. None of those results showed low strength nor an unusual stress path that could be attributed to cracking during saturation. This is manifested by a linear failure envelope in the effective radial stress range between approximately 2–13 MPa (Fig. 13).

Opalinus Clay from an even shallower depth (borehole Lausen, < 50 m) was tested by[9] and[15]. In the first, samples were saturated at various stress levels, between 1.3 and 16.9 MPa. An exponentially increasing swelling strain was recorded as a function of decreasing confinement at which saturation was performed. Samples saturated at the lowest confinement showed swelling due to saturation on average of 1.4 %. The swelled samples showed low strength compared to the expected trend. The authors attributed this to potential microfissuring due to saturation, which has been earlier observed on similar clay-rocks such as the Callovo Oxfordian claystone[1]. In[15], samples were left in equilibrium with high relative humidity (92 %-98 %). However, the authors report these RH values to be close to the native activity of the samples (~91 %) and no weight gain was observed, which suggests no significant swelling. The test results do not show signs of damage, and a linear Mohr-Coulomb failure envelope could be deduced. These observations also point towards a linear failure envelope[15], except where results at low effective stress are related to excessive swelling and damage[9] .

### 4.6. Comparison with caprock shales

From a dataset of over 90 caprock shales tested adopting the alternative procedure, 6 were extracted and compared with the Opalinus Clay response. The six shales are identified as shale A, B, C, E, G and H[10, 12,13], feature a porosity range of ~12 % to ~30 %, and a clay mineral content between 65 wt% and 76 wt%. These shales have a porosity similar to or higher than that of Opalinus Clay (in the TBO ~10–12 %) and clay mineral contents in the upper part of the range observed for Opalinus Clay, or higher.

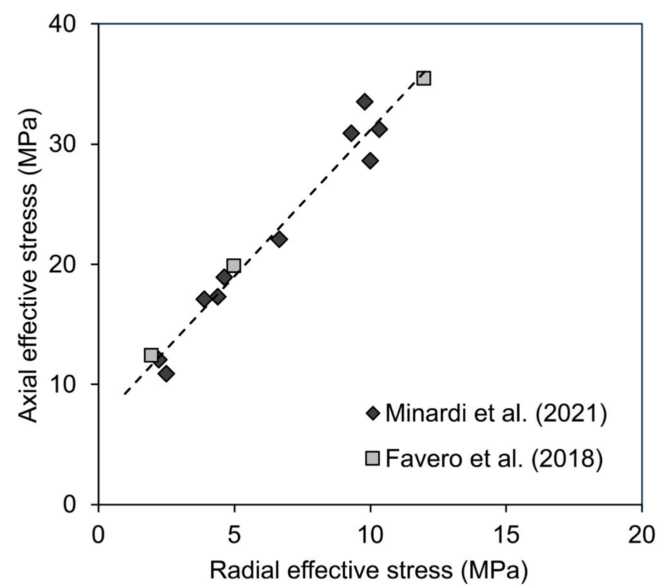


**Fig. 13.** Good agreement of Opalinus Clay test results from Mont Terri URL and linear failure envelope indicates that no sample damage from excessive swelling occurred. Results are from Favero et al.,[14] and Minardi et al.[18].

Results of these shales show a response similar to that of Opalinus Clay. When subjected to high swelling during the saturation/preconditioning phase and this is not compensated by the compression in the cell during the pre-shearing phase, samples often showed low strength. Again, the specimens exposed to very low confinement exhibit a relevant decrease in strength, which is not compatible with the observed linear failure envelope of these shales. Expanding upon the example results shown in Ewy et al.,[10], complete results are plotted in Fig. 14. Lower strength was not observed for any Shale A samples, even those equilibrated to 98 % RH. For Shales B and C, equilibration at 98 % RH resulted in lower strength but 96 % RH did not. For Shale G,

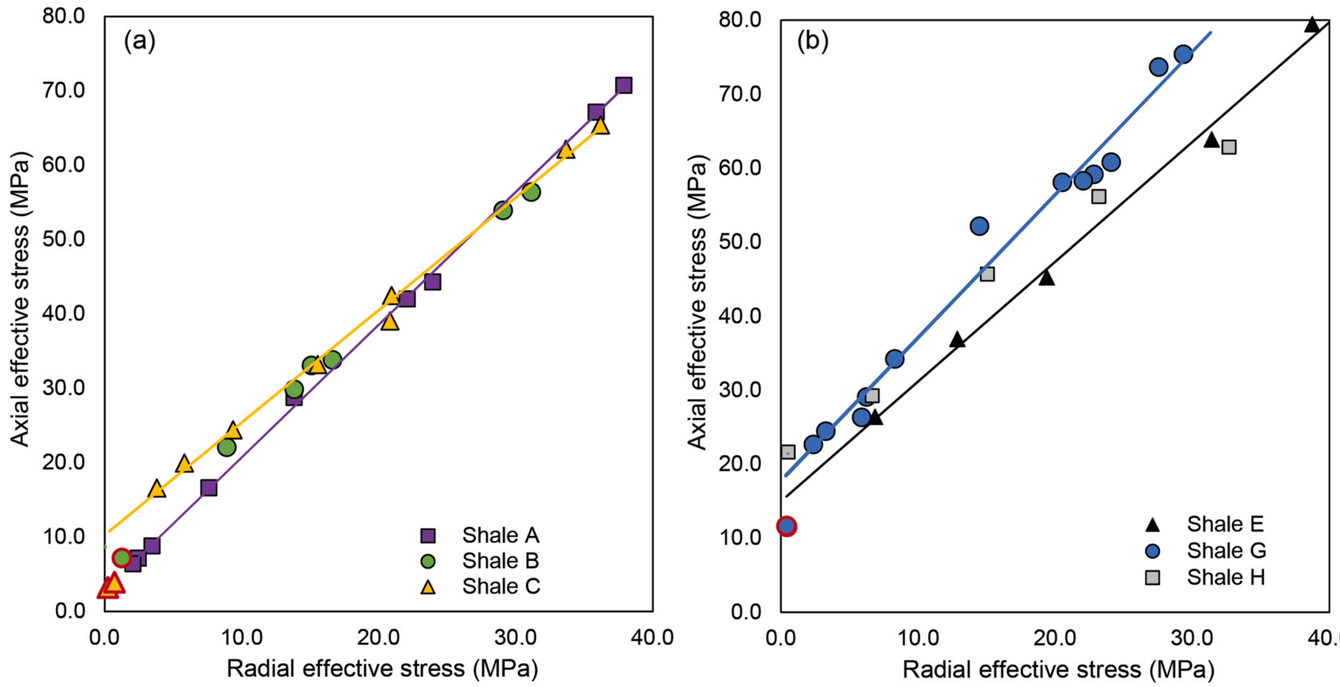


**Fig. 14.** Extended results from[10] on various caprock shales. Linear failure envelope in the radial versus axial effective stress. Red marker lines indicate damaged samples, deviating from the linear failure trend as constrained on test results across the entire radial effective stress range.

equilibration at 96 % RH resulted in lower strength but 92 % did not. Of these four shales, A has the highest porosity (~0.30) and a high native-state RH of at least 96 %, whereas Shale G is lower porosity (~0.18) and has a native-state RH of only ~80 %[12,13].

Fig. 15 reports the volumetric strain during saturation (in a controlled-RH desiccator) against the volumetric strain at the start of shear for caprock shales. Samples which yielded results out of the failure envelope (Fig. 14) are highlighted with a red marker line. For those, the effective minimum radial stress during shearing (at max pore pressure) is indicated. All those low-strength samples experienced both high swelling during preconditioning/testing and low (<1 MPa) minimum radial confinement.

For these shales, a higher amount of swelling could generally be accommodated by the shale structure without impacting the material strength response; several samples experienced swelling strains of −0.01 to −0.02 during preconditioning and did not exhibit reduced strength. This is to be attributed to the generally higher porosity and high clay content, i.e. a more ductile response, which can likely accommodate larger deformations potentially with limited formation of fissures. Several of these samples experienced somewhat low minimum radial stress during shearing (at maximum pore pressure), although it was generally higher than 2 MPa.

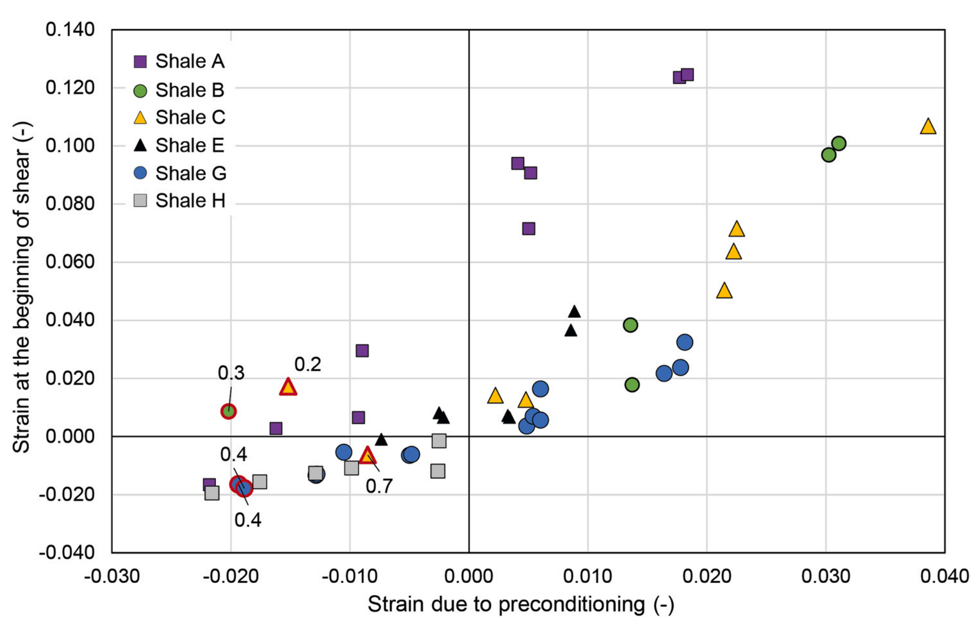


**Fig. 15.** Volumetric strain during saturation versus volumetric strain at beginning of shear for caprock shales A, B, C, E, G, H ([10,12,13]). Samples with a red marker line correspond to those with lower strength in Fig. 14, and the label indicates the effective minimum radial stress during shearing (at max pore pressure). Notet that effective radial stress in all other tests was generally greater than 2 MPa.

## 5. Conclusions and recommendations for testing

The results presented in this contribution demonstrate that sample preparation and testing techniques have an impact on the mechanical response of shales at low effective confinement. These could lead to both a misestimation of the geomaterial mechanical parameters and misinterpretation of the behaviour, e.g. strength evolution with confinement. In particular, failure envelopes at low effective stress might show an apparent non-linearity due to sample damage at low effective stress.

Core storage and sample preparation usually lead to a certain desaturation, which needs to be corrected prior to the shear phase in triaxial testing. Good saturation is important to track effective stress.

Since the swelling can induce not only a volumetric expansion but also localised fissuring, isochoric saturation might be a suitable option for saturating shales. Taking into account the maximum estimated stress state experienced by the material can help to set a limit to the maximum stress that might be reached during this phase. As shown, shales can sustain some expansion, but large expansion at low effective stress must be prevented, as this can lead to irreversible damage and affect the mechanical behaviour. If the water content must be significantly increased prior to sample mounting by use of a RH desiccator, physical restraint perpendicular to bedding (e.g. by use of clamps) is recommended in order to limit the swelling strain.

Swelling (strain and pressure) developed during saturation depends on the depth of core recovery, and the amount of drying of the material experienced during core extraction, storage and sample preparation. Minimising said drying will limit the strain or pressure development during the saturation phase.

Lower porosity shales, such as Opalinus Clay, and lower clay content shale are expected to be more prone to fissuring during swelling, because of the more relevant diagenetic cementation. For Opalinus Clay at siting regions for a deep geological repository, volumetric (swelling) strains <-1 vol% during saturation may be associated with damage to material properties.

Shales with higher porosity and/or higher clay content as those shown for some caprock shales, indicate ranges of acceptable volumetric strains up to −2 %.

In case high swelling occurred during test phases, loading to higher confinement before reaching the target stress state for shearing appears to reduce the effect of generated fissures on the mechanical response, possibly by improving the interlocking of grains across the fissure.

Generally, higher confinement contributes to keeping the fissures mechanically closed, hence less prone to drive the sample failure. A minimum confinement during all phases of testing is therefore to be preferred. Nonetheless, small effective confining stress is not associated with damage if samples were subjected to limited swelling (thus, limited to no fissuring).

## Declaration of Competing Interest

The authors declare that they have no known competing financial interests or personal relationships that could have appeared to influence the work reported in this paper.

## Data availability

Data will be made available on request.

## Acknowledgements

This study was funded by the National Cooperative for the Disposal of Radioactive Waste (Nagra), Switzerland. The authors greatly acknowledge the support of Dr Eleni Stavropoulou in the elaboration of the micro CT scanned samples. The compression tests were performed at RSTD, NGI and Sintef laboratories, and we are particularly grateful for the efforts of R. Stankovic, K. Halvorsen, M. Soldal and J. Stenebråten. Data on caprock shales for Section 4.6 were provided by the University of Texas GeoFluids Consortium; tests were originally performed at Chevron and RSTD.

## Appendix

Table A1 includes, together with the ID and the procedure adopted (refer to Table 2 for the details), the water content before and after the RH equilibrium, the volumetric strain due to RH equilibrium, and the cumulated strains up to the start of shear, the minimum radial effective stress achieved during shearing (once the maximum pore pressure is achieved), and the ratio between maximum mean effective confinement achieved before shearing and the mean effective stress at start shear, and the classification damaged/undamaged (D/U).

**Table A1**
Water content at sample as prepared and at the RH equilibrium, volumetric strain (compression positive) due to RH equilibrium and at start of shear, minimum radial effective stress confinement during shearing, ratio of the maximum effective mean stress achieved before the shear phase ( $p'_{max}$), and the effective mean stress at the start of the shear phase ($p'_0$). Classification (D= damaged, U= undamaged). All samples. *Testing procedure details in Table 2.

| ID | Procedure | Water content | | Volumetric strain | | σ'r,min | Ratio p'max/p'0 | D/U |
|---|---|---|---|---|---|---|---|---|
| | | Sample as prepared [-] | At RH equilibrium [-] | Due to RH equilibrium [-] | Up to shear start [-] | MPa | [-] | |
| A4_TRU1_1 | C | 0.047 | | | −0.0033 | 1.14 | 3.8 | U |
| B2_TRU1_1 | C | 0.050 | | | −0.0018 | 2.05 | 1.4 | U |
| B7_TRU1_1 | C | 0.049 | | | −0.0045 | 1.03 | 3.3 | U |
| C4_TRU1_1 | A | 0.044 | 0.051 | −0.014 | 0.0003 | 0.32 | 1.2 | D |
| C5_TRU1_1 | A | 0.043 | 0.048 | −0.015 | −0.0059 | 1.75 | 1.0 | U |
| A8_TRU1_1 | C | 0.045 | | | −0.0037 | 0.67 | 3.5 | U |
| A10_TRU1_1 | C | 0.052 | | | −0.0041 | 0.53 | 3.4 | U |
| A11_TRU1_1 | C | 0.044 | | | −0.0049 | 5.00 | 5.7 | U |
| C13_BOZ1_1 | A | 0.038 | 0.046 | −0.007 | 0.0057 | 1.53 | 1.0 | U |
| C1_BOZ1_1 | A | 0.044 | 0.048 | −0.007 | 0.0066 | 4.58 | 1.0 | U |
| C3_BOZ1_1 | A | 0.042 | 0.046 | −0.006 | 0.0005 | 0.96 | 1.0 | U |
| C5_BOZ1_1 | A | 0.047 | 0.050 | −0.006 | 0.0138 | 3.77 | 1.0 | U |
| C7_BOZ1_1 | A | 0.046 | 0.051 | −0.011 | −0.0045 | 0.61 | 1.0 | D |
| C12_BOZ1_1 | A | 0.043 | 0.048 | −0.013 | −0.0059 | 6.46 | 1.0 | U |
| A1_BOZ1_1 | C | 0.050 | | | −0.0026 | 0.60 | 3.7 | U |

(continued on next page)

**Table A1** (*continued*)

| ID | Procedure | Water content | | Volumetric strain | | σ'r,min | Ratio p'max/p'0 | D/U |
|---|---|---|---|---|---|---|---|---|
| | | Sample as prepared [-] | At RH equilibrium [-] | Due to RH equilibrium [-] | Up to shear start [-] | MPa | [-] | |
| A2_BOZ1_1 | C | 0.050 | | | −0.0013 | 5.98 | 3.7 | U |
| A8_BOZ1_1 | C* | 0.051 | | −0.018 | −0.0116 | 0.38 | 1.0 | D |
| A5_BOZ1_1 | C | 0.052 | | | 0.0071 | 0.59 | 2.8 | U |
| A6_BOZ1_1 | C | 0.052 | | | −0.0021 | 3.03 | 2.0 | U |
| A9_BOZ1_1 | C* | 0.044 | | −0.008 | −0.0096 | 0.79 | 1.5 | U |
| A10_BOZ1_1 | C | 0.048 | | | −0.0080 | 1.10 | 5.1 | U |
| A11_BOZ1_1 | C* | 0.049 | | −0.011 | 0.0084 | 0.60 | 2.9 | U |
| C5_MAR1_1 | A | 0.052 | 0.055 | −0.009 | 0.0009 | 3.33 | 1.0 | U |
| C7_MAR1_1 | A | 0.054 | 0.060 | −0.007 | 0.0120 | 0.26 | 1.0 | D |
| B1_MAR1_1 | C | 0.065 | | | −0.0021 | 1.93 | 2.5 | U |
| B2_MAR1_1 | C | 0.045 | | | −0.0047 | 4.99 | 3.7 | U |
| C1_MAR1_1 | A | 0.047 | 0.052 | −0.015 | 0.0008 | 3.60 | 1.0 | U |
| C3_MAR1_1 | A | 0.047 | 0.053 | −0.013 | 0.0000 | 0.12 | 1.0 | D |
| C11_MAR1_1 | A | 0.048 | 0.055 | −0.014 | −0.0075 | 4.94 | 1.0 | U |
| C11_BOZ2_1 | A | 0.035 | 0.042 | −0.015 | −0.0081 | 1.13 | 2.7 | D |
| C6_BOZ2_1 | A | 0.039 | 0.044 | −0.009 | 0.0147 | 3.92 | 1.0 | U |
| C5_BOZ2_1 | A | 0.036 | 0.044 | −0.014 | 0.0028 | 1.47 | 1.0 | D |
| C12_BOZ2_1 | A | 0.035 | 0.042 | −0.001 | 0.0037 | 0.00 | 2.5 | U |
| C1_BOZ2_1 | A | 0.042 | 0.049 | −0.012 | −0.0070 | 0.71 | 1.0 | D |
| C2_BOZ2_1 | A | 0.046 | 0.051 | −0.012 | 0.0027 | 4.24 | 1.0 | D |
| C7_BOZ2_1 | A | 0.042 | 0.049 | −0.011 | 0.0015 | 1.40 | 2.2 | U |
| C9_BOZ2_1 | A | 0.040 | 0.044 | −0.005 | 0.0017 | 5.16 | 2.0 | U |
| B12_BOZ2_1 | A | 0.053 | 0.058 | −0.013 | −0.0140 | 0.78 | 1.0 | D |
| B1_BOZ2_1 | C | 0.058 | | | −0.0043 | 0.91 | 2.9 | U |
| B2_BOZ2_1 | C | 0.057 | | | −0.0004 | 3.36 | 1.5 | U |
| C3_BOZ2_1 | A | 0.050 | 0.057 | −0.011 | −0.0039 | 0.42 | 1.0 | D |
| C4_BOZ2_1 | A | 0.045 | 0.050 | −0.007 | −0.0009 | 1.94 | 1.0 | U |
| C8_BOZ2_1 | A | 0.047 | 0.054 | −0.003 | 0.0110 | 1.04 | 2.4 | U |
| C10_BOZ2_1 | A | 0.048 | 0.052 | −0.003 | 0.0039 | 0.29 | 4.2 | U |

The artificial porewater (APW) used in the geomechanical tests is based on the recipe derived from the investigations in the Schlattingen borehole[21], and the composition is reported in Table B1. This recipe defines a porewater saturated with respect to calcite and dolomite under atmospheric CO2 partial pressure (lab conditions).

**Table B1**
Artificial pore water recipe.

| Compound | mmol/$kg_{H2O}$ | g/$kg_{H2O}$ |
|---|---|---|
| NaCl | 115.26 | 6.7356 |
| $NaHCO_3$ | 0.54 | 0.0456 |
| $CaCl_2$ 2 $H_2O$ | 11.91 | 1.7510 |
| KCl | 2.55 | 0.1902 |
| $MgCl_2$ 6 $H_2O$ | 9.17 | 1.8635 |
| $Na_2SO_4$ | 24.00 | 3.4089 |

## References


1. Bornert M, Valès F, Gharbi H, Nguyen Minh D. Multiscale full-field strain measurements for micromechanical investigations of the hydromechanical behaviour of clayey rocks. *Strain*. 2010;46:33–46. https://doi.org/10.1111/j.1475-1305.2008.00590.x.
2. Crisci, E., 2019. Hydro-mechanical response of Opalinus Clay shale: dependency on composition and burial depth. EPFL thesis. https://doi.org/10.5075/epfl-thesis-7421.
3. Crisci E, Ferrari A, Laloui L. Discussion on "Experimental Deformation of Opalinus Clay at Elevated Temperature and Pressure Conditions: Mechanical Properties and the Influence of Rock Fabric" of Schuster, V., Rybacki, E., Bonnelye, A., Herrmann, J., Schleicher, A.M., Dresen, G. *Rock Mech Rock Eng*. 2022;55:463–465. https://doi.org/10.1007/s00603-021-02654-1.
4. Crisci E, Giger SB, Laloui L, et al. Insights from an extensive triaxial testing campaign on a shale for comparative site characterization of a deep geological repository. *Geomech Energy Environ 38*. 2024, 100508. https://doi.org/10.1016/j.gete.2023.100508.
5. Crisci, E., L. Laloui and Giger, S. TBO Trüllikon-1-1: Data Report, Dossier IX Rock-mechanical and geomechanical laboratory testing. 2021. (Nagra Arbeitsbericht NAB 20-09 Rev.1).
6. Crisci E., Laloui L., Giger S. TBO Marthalen-1-1: Data Report, Dossier IX Rock-mechanical and geomechanical laboratory testing. 2021. (Nagra Arbeitsbericht NAB 21-20).
7. TBO Bözberg-1-1: Data Report, Dossier IX Rock-mechanical and geomechanical laboratory testing. 2022. (Nagra Arbeitsbericht NAB 21-21).
8. TBO Bözberg-2-1: Data Report, Dossier IX Rock-mechanical and geomechanical laboratory testing. 2022. (Nagra Arbeitsbericht NAB 21-22).
9. Delage P, Belmokhtar M. Drained triaxial testing of shales: insight from the Opalinus Clay. *Acta Geotech*. 2022;17:2855–2874. https://doi.org/10.1007/s11440-021-01395-3.
10. Ewy R, Dirkzwager J, Bovberg C. Claystone porosity and mechanical behavior vs. geologic burial stress. *Mar Pet Geol*. 2020;121, 104563. https://doi.org/10.1016/j.marpetgeo.2020.104563.
11. Ewy RT. Practical approaches for addressing shale testing challenges associated with permeability, capillarity and brine interactions. *Geomech Energy Environ, Theme Issue Sel Pap Int Workshop Adv Lab Test Model Soils Shales*. 2018;14:3–15. https://doi.org/10.1016/j.gete.2018.01.001.
12. Ewy RT. Shale/claystone response to air and liquid exposure, and implications for handling, sampling and testing. *Int J Rock Mech Min Sci*. 2015;80:388–401. https://doi.org/10.1016/j.ijrmms.2015.10.009.
13. Ewy RT. Shale swelling/shrinkage and water content change due to imposed suction and due to direct brine contact. *Acta Geotech*. 2014;9:869–886. https://doi.org/10.1007/s11440-013-0297-5.
14. Favero V, Ferrari A, Laloui L. Anisotropic behaviour of opalinus clay through consolidated and drained triaxial testing in saturated conditions. *Rock Mech Rock Eng*. 2018;51:1305–1319. https://doi.org/10.1007/s00603-017-1398-5.
15. Giger SB, Ewy RT, Favero V, Stankovic R, Keller LM. Consolidated-undrained triaxial testing of Opalinus Clay: Results and method validation. *Geomech Energy*

*Environ, Theme Issue Sel Pap Int Workshop Adv Lab Test Model Soils Shales*. 2018;14: 16–28. https://doi.org/10.1016/j.gete.2018.01.003.
16. Mazurek M, Hurford AJ, Leu W. Unravelling the multi-stage burial history of the Swiss Molasse Basin: integration of apatite fission track, vitrinite reflectance and biomarker isomerisation analysis. *Basin Res*. 2006;18:27–50. https://doi.org/10.1111/j.1365-2117.2006.00286.x.
17. Menaceur H, Delage P, Tang AM, Talandier J. The status of water in swelling shales: an insight from the water retention properties of the callovo-oxfordian claystone. *Rock Mech Rock Eng; Wien*. 2016;49:4571–4586. https://doi.org/10.1007/s00603-016-1065-2.
18. Minardi A, Giger SB, Ewy RT, et al. Benchmark study of undrained triaxial testing of Opalinus Clay shale: Results and implications for robust testing. *Geomech Energy Environ*. 2021;25, 100210. https://doi.org/10.1016/j.gete.2020.100210.
19. Voltolini M, Ajo-Franklin JB. The sealing mechanisms of a fracture in opalinus clay as revealed by in situ synchrotron x-ray micro-tomography. *Front Earth Sci*. 2020;8.
20. Wang LL, Bornert M, Héripré E, Yang DS, Chanchole S. Irreversible deformation and damage in argillaceous rocks induced by wetting/drying. *J Appl Geophys*. 2014;107: 108–118. https://doi.org/10.1016/j.jappgeo.2014.05.015.
21. Wersin, P., Mazurek, M., Waber, H.N., Mäder, U.K., Gimmi, T., Rufer, D., de Haller, A., 2013. Rock and porewater characterisation on drillcores from the Schlattingen borehole (No. NAB 12-54). Institute of Geological Sciences, University of Bern; Nagra.